



22nd Annual International Symposium
October 22-24, 2019 | College Station, Texas

Impact of water on toxic hydrogen fluoride generation from the decomposition of LiPF₆ in lithium-ion battery electrolytes

Ji Yun Han,^{1*} Jeongwook Seo,²⁺ Seungho Jung,^{3*}
*Ajou University

⁺Samsung Electronics Co., Ltd.

¹ Department of Environmental and Safety Engineering, Ajou University, Suwon, 16499, Korea

² Samsung Electronics Co., Ltd., Suwon, Korea

*Presenter E-mail: jy0324han@ajou.ac.kr

Abstract

Toxic hydrogen fluoride (HF) gas can be generated when LiPF₆, a salt used in lithium-ion battery electrolytes, thermally decomposes and/or reacts with trace water. Simultaneous thermal analysis and mass spectrometry (STA-MS) was conducted on five different organic solvents containing LiPF₆ to determine the temperatures at which HF is generated and the activation energies of the decomposition reaction. STA-MS allows the simultaneous direct observation of electrolyte thermal stability and hydrogen fluoride generation, something that is not possible with gas chromatography–mass spectrometry alone, thus it represents a more efficient and simple experimental approach.

The five solvents tested in this study were anhydrous tetrahydrofurfuryl alcohol (THFA), 1,3-dioxolane (1,3-DL), diethyl carbonate (DEC), 1,2-dimethoxyethane (DME), and ethyl carbonate (EC). STA-MS analysis of the LiPF₆ in these solvents revealed that HF generation occurred at different temperatures for each electrolyte. In the case of 1M LiPF₆ in THFA, the addition of 1000 ppm of water reduced the thermal decomposition temperature compared to solid neat LiPF₆. Except for EC, all of the other electrolyte systems exhibited a lower HF generation temperature and a lower reaction activation energy (E_a) when water was present. Additionally, from a risk assessment perspective, the results indicate that the HF generation starts from the SEI layer decomposition stage which occurs early in the thermal runaway mechanism of the lithium-ion battery.

This research can be used to develop more thermally stable and safer electrolytes in the future, especially with respect to HF generation. In addition, this study highlights the need for research into measures to combat large-capacity lithium-ion battery fires, which may occur in electric vehicles and grid-scale energy storage systems.

Keywords: lithium-ion battery, electrolytes, fire, toxic gases, STA-MS experiment, thermal characteristics of Li-ion battery electrolytes, risk of HF gas.

Introduction

Lithium-ion batteries represent a type of rechargeable electrochemical energy storage system in which energy is charged and discharged by the transfer of lithium ions. During the discharge process, intercalated lithium ions are released from the anode and transferred to the cathode via an electrolyte. The reverse occurs during charging—the lithium ions are re-intercalated into the anode via an externally applied potential. During each charge and discharge cycle, a portion of the lithium ions are immobilized and can no longer participate in the charge–discharge process which leads to a loss of battery capacity over time.

The three most important characteristics of industrial and commercial lithium-ion batteries are their energy density, cycle life, and capacity retention. Energy density is the normalized amount of energy that is available from a battery and is calculated as either the available energy per unit of battery mass or as the available energy per unit of battery volume. The lithium-ion battery cycle life represents how many charge and discharge cycles the battery can perform before the remaining capacity is no longer sufficient for a given application. Capacity retention is how much of the initial or specified capacity (i.e., the amount of energy that can be stored in the battery) is left after a certain number of charge and discharge cycles. Currently, a lithium-ion battery cycle life is over 1500 cycles, with a capacity retention of over 85% of the initial discharge capacity (Ramanujapuram et al., 2016).

The advances in cycle lifetime and energy density over the past decade have attracted societal and industrial attention and have made it possible for these batteries to be employed in various applications, ranging from mobile phones to electric vehicles. In addition, rapidly growing renewable energy industries, such as wind, solar, and smart grid systems, require large-scale energy storage systems (ESSs) in the range of 3–20 MWh, for which lithium-ion batteries are considered the optimal technology (Park et al., 2018).

However, the high-energy storage capability of lithium-ion batteries also comes with some notable risks. For example, higher energy density and greater performance requirements have also increased the possibility of thermal runaway scenarios. Seven ESS fires have occurred in South Korea since 2017, leading to property losses of approximately 17 million US dollars. The South Korean government recently conducted an investigation into the cause of these ESS fires and published a report on their findings (Park et al., 2018).

Lithium-ion battery fires are not limited to large-scale ESS and have become a more frequent event globally. A U.S. Department of Transportation investigation report stated that there were 265 air/airport incidences involving lithium/lithium-ion batteries being carried onboard as cargo or baggage. In fact, 42% of all incidents (112 incidents) occurred in the 3 most recent years spanning from 2017 to July 2019 (FAA Office of Security and Hazardous Materials Safety, 2019). These incidences were not limited to a certain battery product or the specific industries that utilize them. As a result, the issue of lithium-ion battery safety has become a serious topic of interest, especially as large battery fires, such as those from EV or ESS battery packs, cannot be easily extinguished and result in unstoppable fires in most cases.

Table 1. Examples of recent lithium-ion battery-related incidents (from Feng et al., 2018; Park et al., 2018; FAA Office of Security and Hazardous Materials Safety, 2019).

Date	Industry	Device (if application)	Location	Incident summary and probable cause
July 2019	Airline	Laptop / Tablet	US	A Unit Load Device (ULD) at JFK Airport produced smoke and caught on fire after external impact, internal short circuit
Jun. 2019	Airline	Cell Phone	US	A passenger's phone produced smoke and caught on fire, internal short circuit
May 2019	Airline	E-cigarette and spare battery	US	While loading baggage on DL flight 880 to Minneapolis, MN (MSP), a bag on the belt loader produced smoke and caught on fire, internal short circuit
Jun. 2018	Solar	19 MWh ESS	Gunsan, S. Korea	30 min after a full charge of the ESS, fire started on Rack No. 13 of the ESS, cause unknown
Aug. 2017	Wind	17 MWh ESS	Gochang, S. Korea	Fire started at ESS pack during summer time due to failure of the HVAC thermal management system, thermal abuse conditions created by HVAC failure
July 2016	EV	EV bus	Nanjing, China	The battery pack of an EV bus caught fire after heavy rain. Water immersion caused short circuit.
Apr. 2015	EV	EV bus	Shenzhen, China	Wuzhou Dragon EV bus caught fire during charging in a garage, overcharging of battery pack

The hazards of lithium-ion batteries, including thermal runaway scenarios, are closely related to the materials that compose the batteries. For example, when the LiPF_6 salt, the most commonly used salt in the lithium-ion battery electrolytes, decomposes to form LiF and PF_5 , the PF_5 acts as a catalyst in the decomposition reaction of the electrolyte solvent (Lisbona et al., 2011; Abraham et al., 2006).

Thermal runaway in lithium-ion battery has been the focus of many recent studies. In these studies, the mechanisms responsible for lithium-ion battery fires have been investigated using accelerating rate calorimetry (ARC), differential scanning calorimetry (DSC), and isothermal microcalorimetry IMC (Inoue and Mukai, 2017). Liu et al. reported that there are various side reactions during the charge and discharge cycle of a lithium-ion battery in the solid electrolyte interface (SEI) layer on the surface of the anode and cathode that contribute to thermal runaway scenarios (Liu et al., 2014). Under thermal runaway situations, the heat generated will lead to decomposition of the lithium-ion battery electrolyte.

Most commercial lithium-ion batteries contain electrolytes consisting of LiPF₆ salt in an organic solvent mixture. This type of electrolyte is characterized by high conductivity, good electrochemical stability, and the ability to work at low temperatures. However, the thermal stability is poor. It is well known that LiPF₆ salt in the organic solvent of lithium-ion battery electrolytes can produce toxic hydrogen fluoride (HF) gas as a thermal decomposition reaction product (Gaulupeau., 2017). Larsson et al. have also reported gas generation due to electrolyte decomposition reactions and assessed the toxicity of the HF gas produced by LiPF₆ decomposition in the presence of water (Michalak, 2015; Wang, 2018; Larsson et al., 2017). LiPF₆ decomposition reactions are shown in Equations 1 to 3 where: Equation 1 is the anhydrous thermal decomposition of LiPF₆ salt, Equation 2 is the HF generation reaction of PF₅ (the product of Equation 1) with water (H₂O), and Equation 3 is the HF generation reaction of LiPF₆ salt in the presence of water (Larsson et al., 2017).



Larsson et al. reported that the immediately dangerous to life or health (IDLH) level for HF is 0.025 mg/m³ (30 ppm) and the 10-minute lethal concentration is 0.0139 g/m³ (170 ppm) (Larsson et al., 2017). As a result, HF gas emitted from a fire involving a lithium-ion battery that operates in the range of kWh to MWh (the class used in electric vehicles) can be very dangerous and poses serious health risks (Larsson et al., 2017).

In this study, a new method to measure and analyze electrolyte stability using simultaneous thermal analysis–mass spectrometry (STA-MS) is presented, with a focus on HF gas generation. The association between the five different electrolyte stabilities and their activation energy, the generation of HF gas, and the effect of the addition of trace water is also reported.

Experiment

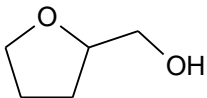
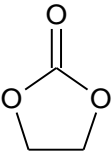
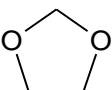
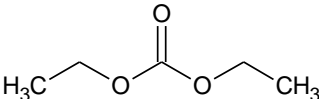
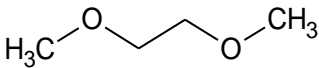
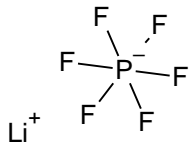
Five organic solvents were used to create 1 M electrolytes containing LiPF₆ salt. The electrolyte decomposition conditions were assessed using STA-MS in order to determine the thermal characteristics of the electrolyte solutions. The five solvents used were tetrahydrofurfuryl alcohol (THFA), 1,3-dioxolane (1,3-DL), diethyl carbonate (DEC), 1,2-dimethoxyethane (DME), and ethyl carbonate (EC), all purchased from Tokyo Chemical Industry (TCI). LiPF₆ salt, also purchased from TCI, was dissolved in each solvent to a concentration of 1 M. Two groups of samples were prepared: one containing anhydrous solvents and one containing trace amounts of water (1000 ppm).

The samples were sealed in a hermetic Al₂O₃ crucible pan in a nitrogen-filled box with flowing nitrogen gas to maintain a constant and stable atmosphere. Each of the crucibles was placed in the STA-MS instrument (409 PC and QMS 403C from NETZSCH) and the electrolyte analyzed at temperatures from 35 to 300°C under a constant heating rate of 2°C/min. Thermogravimetry/differential thermal analysis (TG/DTA) results and the MS intensity for the fluorine ion current were recorded by the STA-MS instrument.

Results

The boiling point (bp), flash point (fp), and LiPF_6 decomposition temperatures are presented in Table 2 (Hara et al., 2012; Hess et al., 2015; PubChem, accessed July 22, 2019; Ken et al., 2016; NFPA, 2002). The decomposition temperature of LiPF_6 salt is 181°C , as reported by Xu et al. (2010). As can be seen in Table 2, the electrolyte solvent with the lowest bp is 1,3-DL (75°C) and that with the highest is EC (243°C).

Table 2. Chemical and physical characteristics of the electrolyte materials

Entry	Chemical name	Chemical structure	CAS No.	Molecular weight, g/mol	Boiling point, $^\circ\text{C}$	Flash Point $^\circ\text{C}$	Decomposition, $^\circ\text{C}$
1	Tetrahydrofurfuryl alcohol (THFA)		97-99-4	102.13	178	75	-
5	Ethylene carbonate (EC)		96-49-1	88.06	243	145.5	-
2	1,3-Dioxolane (1,3-DL)		646-06-0	74.08	75	2	-
3	Diethyl carbonate (DEC)		105-58-8	118.13	126 ~ 128	33	-
4	1,2-Dimethoxy ethane (DME)		110-71-4	90.12	85	-2	-
6	Lithium hexafluorophosphate (LiPF_6)		21324-40-3	151.91	-		181 neat (no solvent, solid phase)

The materials characteristic data suggest that, if an internal short or an external heat source were to increase the temperature of a lithium-ion battery to over 75°C , a battery using 1,3-DL as a solvent has an inherent risk of suffering internal damage due to the increase in pressure arising from solvent vaporization. The fp is also an indication of the temperature at which a fire can start if a battery's electrolyte is exposed to oxygen in the ambient air, such as when the protective outer case or pouch is breached by external damage or by the build-up of internal pressure.

Lithium-ion battery safety is strongly associated with environmental factors such as ambient temperature and humidity. When the protective housing of a battery is compromised, ambient humid air can infiltrate the internal components, while moisture can also be introduced into the battery components during production if strict quality control measures are not enforced. When compromised batteries are exposed to an internal short circuit or an external heat source, such as an open flame, any moisture present in the battery poses serious safety risks. In these cases, it is reasonable to expect that HF will be generated due to the thermal decomposition reaction described in the previous section. The presence of moisture can exacerbate this situation because it can affect the thermal decomposition temperature of the salt in the electrolyte.

The DTA spectra and the F⁺ fragments characteristic of the mass spectrum for HF (*m/z* = 19) from the five 1M LiPF₆ electrolyte samples are presented in Figures 1–5. Gaulupeau et al. (2017) reported two characteristic fragments of gaseous HF (F⁺ and HF⁺) that can be used as evidence for the presence of HF. In the present study, F⁺ (*m/z* = 19) was used as an indicator for HF. Equation 3, in which HF is produced as an electrolyte decomposition product, is not significantly affected by the bp of the solvent in each electrolyte. The bp temperatures of THFA and EC were 178°C and 243°C, respectively, which was higher than the other solvents. However, HF generation started at 138°C and 134°C for THFA and EC, respectively, as can be seen in the DTA and HF (*m/z* = 19) mass spectra. In contrast, the same reaction was seen at 150°C, 164°C, and 128°C (and 180°C) for the solvents with a lower bp, 1,3-DL (75°C), DME (85°C), and DEC (126–128°C), respectively, as can be seen in Figures 1–5. This is consistent with a previous study in which it was reported that the solvated form of the Li⁺ cation and the PF₆⁻ anion alters the bp and decomposition reaction temperature (Logan et al., 2018). This phenomenon can also be explained by the activation energy (*E_a*) of the thermal decomposition reactions, which applies to Equation 3 (Yamaki et al., 2015).

Calculation of the Activation Energy

The Kissinger method, which is used to determine the Arrhenius dependence of the rate constant on temperature, is a well-known and relatively reliable method for determining the activation energy (Ahn and Yoon., 2007). According to this approach, in the *n*th reaction system for the *n*th reaction, the rate constant is $K \left(k = A e^{-\frac{E_a}{RT}} \right)$, and the reaction equation in relation to time is as follows:

$$\frac{dx}{dt} = k(1 - x)^n = A e^{-\frac{E_a}{RT}} (1 - x)^n, \quad (4)$$

where *x* represents the conversion rate, *A* is the frequency factor, *E_a* is the activation energy, *R* is the gas constant, and *n* is the order of the reaction.

In most reactions, if *n* is constant, the differential speed of the reaction is 0 at the maximum reaction temperature (*T_p*). This leads to the derivation of the Kissinger equation to calculate the activation energy, as shown in the equation below:

$$\ln \left(\frac{q}{T_p^2} \right) = -\frac{E_a}{R} \left(\frac{1}{T_p} \right) + \ln \left(\frac{R}{E_a} - A \right), \quad (5)$$

where $q = dT/dt$ is the heating rate.

The activation energies for the five electrolytes analyzed in the present study were calculated based on the derived Kissinger equation above. Data from STA-MS were obtained using a constant heating rate of 2°C/min (i.e. $q = 2 \text{ }^\circ\text{C}/\text{min}$), a gas constant of $R = 8.315 \text{ J/Kmol}$, and a frequency factor (A) of 1. The experimentally obtained values from STA-MS were used to calculate the activation energy for each electrolyte. The activation energies were calculated for both the anhydrous form of the electrolytes and the same electrolytes containing trace amounts of water.

Discussion of the STA-MS results

The Equation 3 HF generation temperature and activation energies were calculated and are presented in Table 2. Anhydrous THFA produced a strong HF ($m/z = 19$) ionic current peak at 138°C, as shown in Figure 1c. However, when water was present at 1000 ppm, the HF peak appeared at ~100°C, reaching a maximum at 168°C, and continuing up until 300°C. It is believed that the HF generation temperature is lower due to the lower activation energy in the presence of water, falling from 25.4 kcal/mol to 22.8 kcal/mol.

For EC, the presence of 1000 ppm water did not appear to have a significant impact. As shown in Figure 2b, a single strong endothermic reaction peak was observed regardless of the presence of water. The summit peaks of the HF mass trace ($m/z = 19$) resulting from LiPF_6 decomposition appeared at 128°C and 134°C. The only difference was the faster reaction rate, as illustrated by the difference in the width of the MS peaks for HF. The calculated activation energies were also consistent with these results, as can be seen in Table 3.

Table 3. Comparison of the HF reactions for 1 M LiPF_6 electrolytes with the addition of water (1000 ppm)

Electrolyte solvent (Salt: LiPF_6)	Trace water content (ppm)	HF generation reaction temperature (°C)	Activation energy of HF generation reaction (E_a , kcal/mol)
THFA	None	138	25.4
	1000 ppm	100, 168 (continuous generation from approx. 100 to 300)	22.8, 27.5
EC	None	134	25.1
	1000 ppm	128	24.7
1,3-DL	None	150 (continuous generation from	26.2

		approx. 100 to 300)	
	1000 ppm	120	24.2
DEC	None	128, 180	24.7, 28.3
	1000 ppm	106, 131	23, 24.9
DME	None	164	27.2
	1000 ppm	125 (slowly subsides from 100 to 300)	24.5

For anhydrous 1,3-DL, HF generation reached its maximum at approximately 150°C, and continued to 300°C, as shown in Figure 3c. In the presence of water, however, the HF generation temperature (via Equation 3) was about 30°C lower and the HF peak became narrower and stronger, which suggests that the reaction rate was very rapid. The lowering of the HF generation temperature can be attributed to the lower activation energy (from 26.2 kcal/mol to 24.2 kcal/mol).

With anhydrous DEC, there were two HF generation peaks ($m/z = 19$), which matched the endothermic peaks in Figure 4b: one at 128°C and the other at 180°C. The HF generation at 128°C was minimal compared to that at 180°C. In the presence of 1000 ppm water, there were also two HF ($m/z = 19$) peaks that matched the endothermic peaks. However, these peaks appeared at temperatures that were 22°C and 49°C lower than the peaks observed for the anhydrous DEC. The activation energies were 24.7 and 28.3 kcal/mol without water present and 23.0 and 24.9 kcal/mol with the addition of water (1000 ppm).

For anhydrous DME, HF generation began at approximately 90°C with a small peak, followed by a large peak at 164°C that continued to 300°C, after which the HF ($m/z = 19$) peak slowly subsided (as shown in Figure 5c). In the presence of water, however, the HF generation temperature was lowered to 125 °C, which can be attributed to the lower activation energy (27.2 kcal/mol to 24.5 kcal/mol).

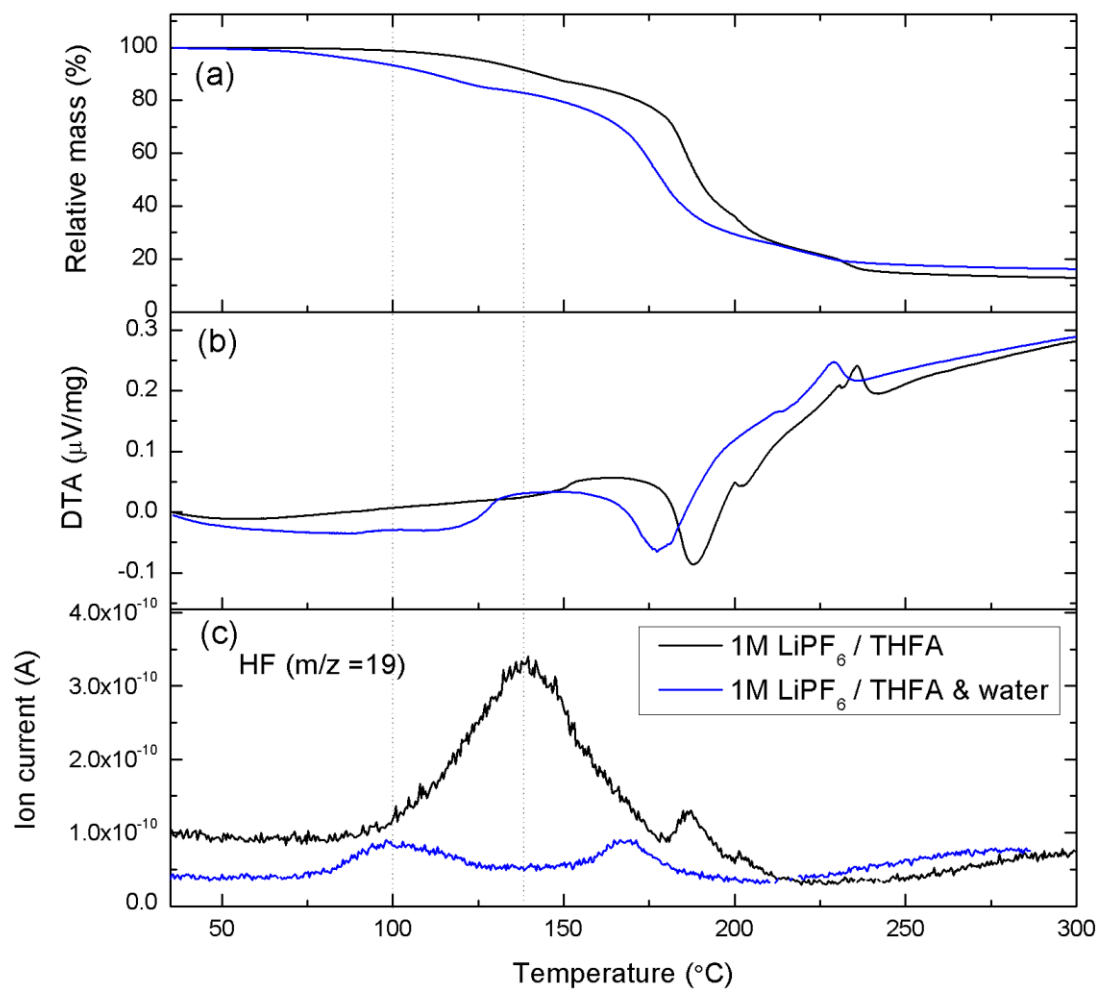


Figure 1. TG/DTA-MS results for the thermal decomposition of the anhydrous 1M LiPF₆/THFA electrolyte (black) and the 1M LiPF₆/THFA electrolyte with 1000 ppm of water added (blue): (a) TGA, (b) DTA, (c) MS.

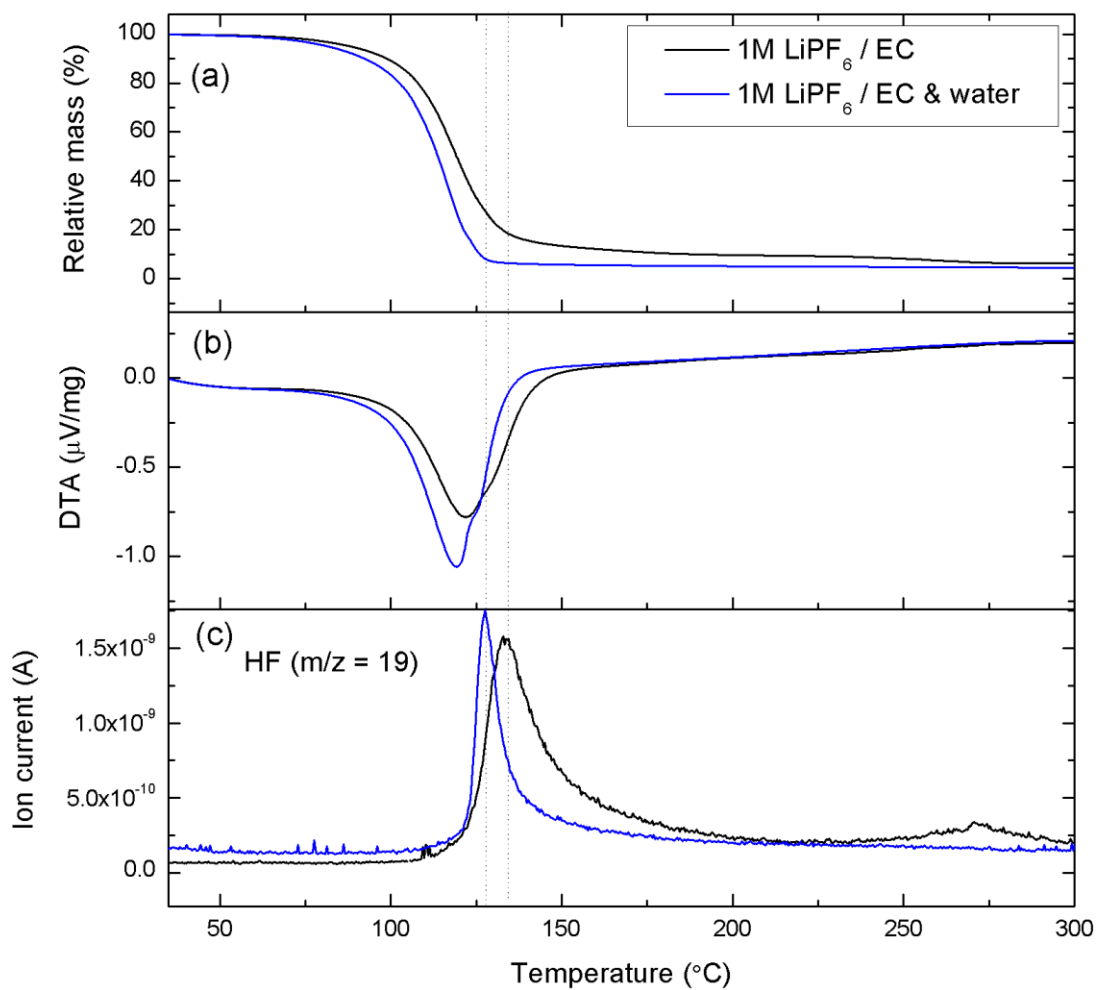


Figure 2. TG/DTA-MS results for the thermal decomposition of the anhydrous 1M LiPF₆/EC electrolyte (black) and the 1M LiPF₆/EC electrolyte with 1000 ppm of water added (blue): (a) TGA, (b) DTA, (c) MS.

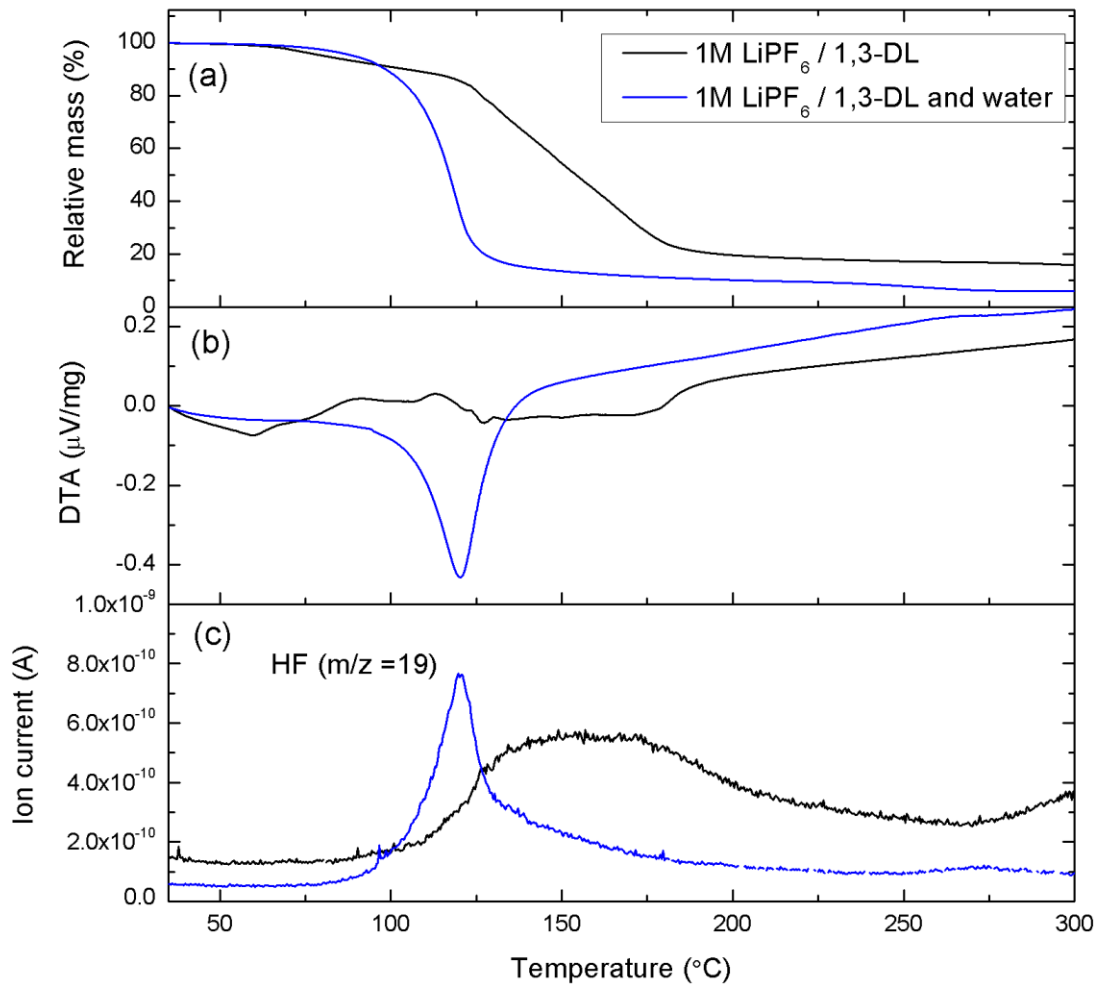


Figure 3. TG/DTA-MS results for the thermal decomposition of the anhydrous 1M LiPF₆/1,3-DL electrolyte (black) and the 1M LiPF₆/1,3-DL electrolyte with 1000 ppm of water added (blue): (a) TGA, (b) DTA, (c) MS.

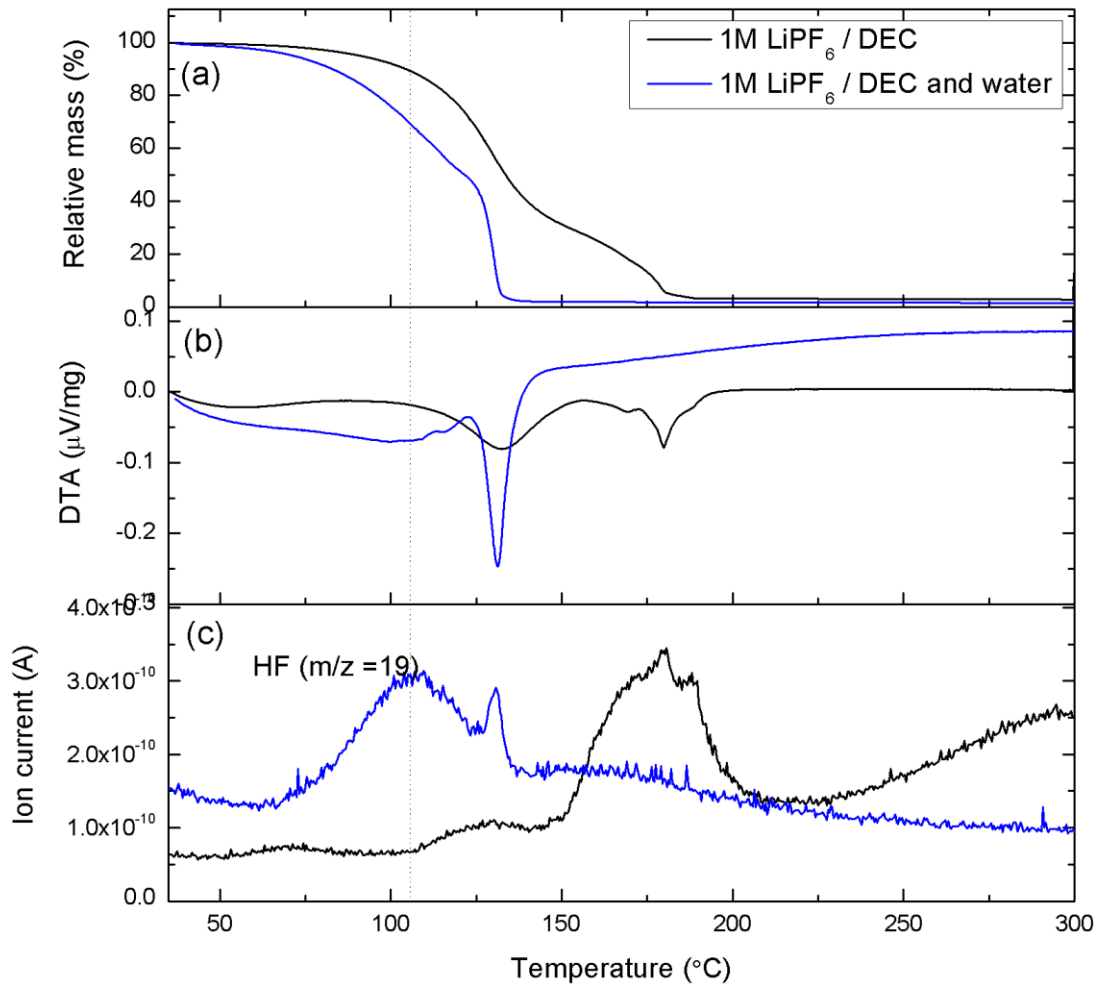


Figure 4. TG/DTA-MS results for the thermal decomposition of the anhydrous 1M LiPF₆/DEC electrolyte (black) and the 1M LiPF₆/DEC electrolyte with 1000 ppm of water added (blue): (a) TGA, (b) DTA, (c) MS.

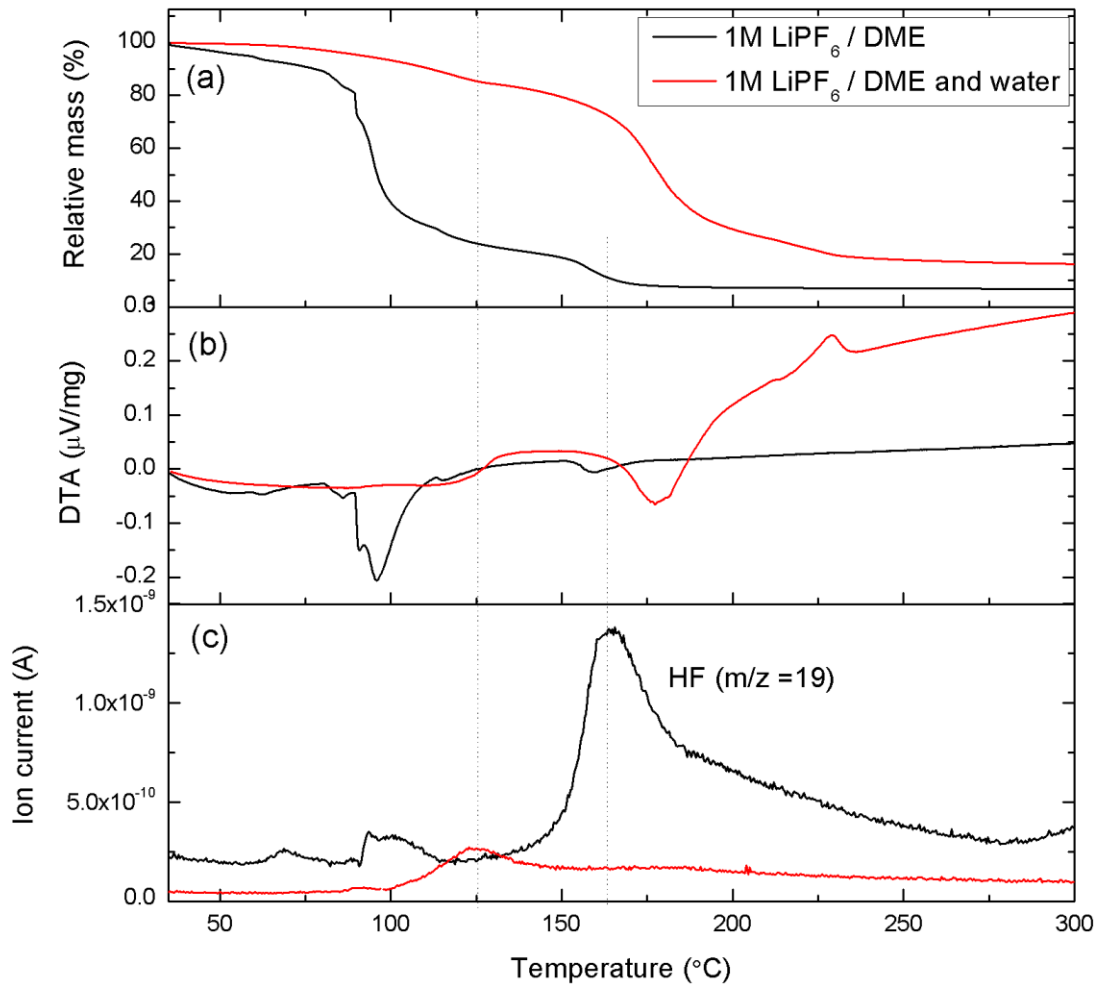


Figure 5. TG/DTA-MS results for the thermal decomposition of the anhydrous 1M LiPF₆/DME electrolyte (black) and the 1M LiPF₆/DME electrolyte with 1000 ppm of water added (red): (a) TGA, (b) DTA, (c) MS.

Risk assessment

Risk assessment for lithium-ion batteries can be broadly categorized into two categories: 1. The assessment of fire or thermal hazards associated with battery thermal runaway scenarios. 2. The assessment of exposure hazards for human inhalation toxicity scenarios due to the toxic gases generated during thermal runaway situations. Both thermal hazard and exposure assessments have been reported by several research teams in recent years (Larsson et al., 2017; Park et al., 2018; Feng et al., 2018). In a recent study, Peng et al. demonstrated that hydrogen fluoride (HF), sulfur dioxide (SO₂), nitric oxide (NO), nitrogen dioxide (NO₂), and hydrogen chloride (HCl) gases are generated during thermal runaway reactions of large-capacity lithium-ion batteries (68 Ah, Pouch type) by studying thermal runaway propagation behaviors. Peng et al. also reported that HF gas exhibited a large range of fractional effective concentrations (FECs)

depending on the state of charge (SOC) of the battery cell: FECs of approximately 40%, 20%, 10%, and 5% for 100%, 75%, 50%, and 0% SOC, respectively. Moreover, Peng et al. highlighted the exposure hazards of HF gas in the toxicity evaluation by exhibiting a maximum concentration of HF at $165 \pm 10 \text{ mg/m}^3$ which is approximately 5.7 times greater than the IDLH value of 24.6 mg/m^3 .

From a thermal hazard perspective, this work has demonstrated that, in the presence of 1000 ppm of water, the temperature of toxic HF gas generation from the decomposition of LiPF_6 is lower than previously considered. In addition, in the presence of 1000 ppm of water, this work has also demonstrated at which stage of the thermal runaway mechanism the toxic HF gas is generated, as shown in Figure 7.

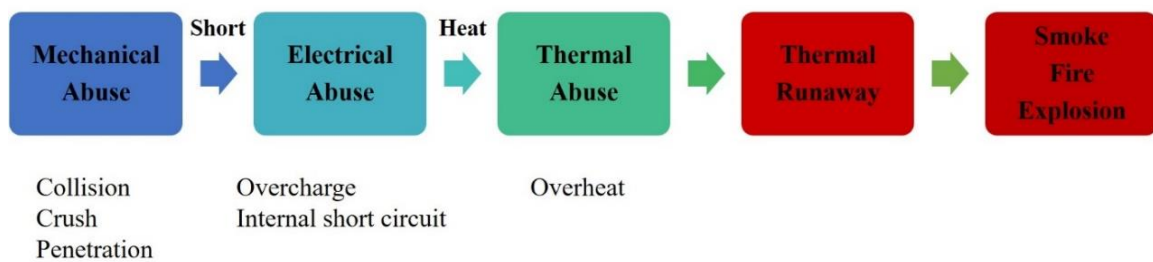


Figure 6. Causes of thermal runaway and lithium-ion battery failure (Feng et al., 2018).

In most thermal runaway mechanism studies, thermal runaway is largely divided into three or four stages with each stage having its own chain exothermic reactions that lead to rapid energy release. (Feng et al., 2018) As reported, the resulting thermal runaway may reach temperatures of up to 500°C very quickly. According to the mechanism described in a study published by Li et al., the SEI layer decomposition is the first to occur before an internal short circuit and the onset temperature is reported to be approximately 90°C at 100% SOC. From there, exothermic reactions between the anode and the electrolyte are initiated up to approximately 200°C . This is followed by separator melting, cathode decomposition, electrolyte decomposition, and, finally, a complete thermal runaway via internal short circuit (Feng et al., 2018; Li et al., 2019).

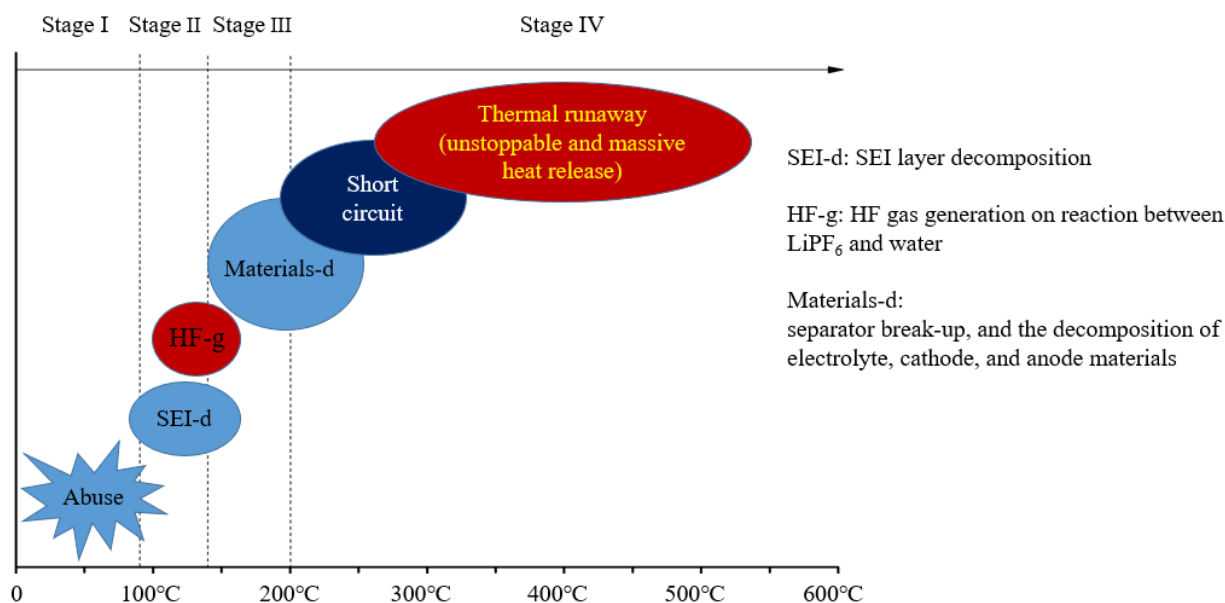


Figure 7. Schematic of thermal runaway mechanism

As previously shown in the TG/DTA-MS results, the presence of water can reduce the temperature at which HF is generated from LiPF_6 decomposition by tens of degrees Celsius depending on the electrolyte solvent. In conjunction with previous studies on the thermal runaway mechanism, it can be inferred that, in the presence of water, toxic HF gas is generated during the early stages of thermal runaway mechanism, namely the SEI layer decomposition, which starts at approximately 90°C, especially for the solvents THFA and DEC. In other solvents tested (EC, 1,3-DL, and DME), the temperature where HF is generated is slightly higher at approximately 120°C.

Conclusions

The presence of water in organic solvent-based electrolytes containing LiPF_6 lowers the temperature at which HF is generated due to the decomposition reaction between LiPF_6 and water. This was observed from the STA-MS analysis of five different electrolyte samples with and without trace amounts of water (1000 ppm). In some cases, the presence of water also accelerated the rate at which HF was generated, as evidenced by the narrower peaks observed in the MS spectra tuned to HF ($m/z = 19$). Of the five electrolytes tested, EC exhibited the smallest change in HF generation temperature in the presence of water. However, large changes in HF generation temperatures and E_a were observed in 1,3-DL, THFA, sDME, and DEC when water was present. The reduction in the HF generation temperature was also observed for the thermal decomposition of LiPF_6 salt in the presence of water. The calculated activation energies were consistent with these observations, with consistently lower activation energies when trace water was present.

In addition, from a risk assessment perspective, the lower HF generation temperature poses a higher risk of exposure as HF can be generated earlier than previously reported. The results indicate that HF gas is generated during the SEI layer decomposition stages at approximately 90°C with THFA showing the lowest generation temperature of 100°C. All other solvents have also been shown to generate HF gas before reaching 150°C.

Additional research is needed to investigate the exact chemical mechanisms responsible for the lowering of the HF generation temperature.

References

Ramanujapuram, Anirudh., Gordon, Daniel., Magasinski, Alexandre., Ward, Brian., Nitta, Naoki., Huang, Cindy, Yushin, Gleb., 2016. Degradation and stabilization of lithium cobalt oxide in aqueous electrolytes. *Energy Environ. Sci*, 9, 1841-1848.

Park, Kwang-Muk., Kim, Jae-Hyun., Park, Jin-Yeong., Bang, Sun-Bae., 2018. A study on the fire risk of ESS through fire status and field investigation. *Fire Sci. Eng*, 32(6), 91-99.

Inoue, Takao, Mukai, Kazuhiko., 2017. Roles of positive or negative electrodes in the thermal runaway of lithium-ion batteries: Accelerating rate calorimetry analyses with an all-inclusive microcell. *Electrochemistry Communications*, 77, 28-31.

Liu, Lin, Park, Jonghyun., Lin, Xianke., Sastry, A. M., Lu, Wei., 2014. A thermal-electrochemical model that gives spatial-dependent growth of solid electrolyte interphase in a Li-ion battery. *J. Power Sources*, 268, 482-490.

Lisbona, D., Snee, T., 2011, A review of hazards associated with primary lithium and lithium-ion batteries. *Process Saf Environ Prot*, 89(6), 434-442.

Abraham, D.P., Roth, E.P., Kostecky, R., McCarthy, K., MacLaren, S., Doughty, D.H., 2006, Diagnostic examination of thermally abused high-power lithium-ion cells. *J. Power Sources*, 161(1), 648-657.

Wang, Aiping., Kadam, Sanket., Li, Hong., Shi, Siqu., Qi, Yue., 2018. Review on modeling of the anode solid electrolyte interphase (SEI) for lithium-ion batteries. *Computational Material*, 4, 15.

Larsson, Fredrik., Andersson, Petra., Blomqvist, Per., Mellander, Bengt-Erik., 2017. Toxic fluoride gas emissions from lithium-ion battery fires. *Scientific Reports*, 7, 10018.

Hess, Steffen., Wohlfahrt-Mehrens, Margret., Wachtler, Mario., 2015. Flammability of li-Ion battery electrolytes: flash point and self-extinguishing time measurements. *J. Electrochem. Soc*, 162 (2) A3084-A3097.

<https://pubchem.ncbi.nlm.nih.gov/compound/7360#section=Melting-Point>.

Ken, Tamamoto., Shigeyuki, Yamada., Masao, Higashi., Tsutomu, Konno., Takashi, Ishihara. 2016. Novel V- and Y-Shaped light-emitting liquid crystals with pentafluorinated bistolane-based luminophores. *Journal of Fluorine Chemistry*, 190, 23-30.

Xu, Mengqing., Xiao, Ang., Li, Weishan., Lucht, Brett L., 2010. Investigation of Lithium tetrafluorooxalato-phosphate [LiPF₄(C₂O₄)] as a lithium-ion battery electrolyte for elevated temperature Performance. *J. Electrochem. Soc*, 157(1), A115-A120.

Logan, E. R., Erin M. Tonita, Gering, K. L., Lin Ma, Michael, K. G., Bauer, Jing Li, L. Y. Beaulieu, and Dahn, J. R., 2018. A study of the transport properties of ethylene carbonate-free Li electrolytes. *J. Electrochem. Soc.*, 165(3), A705-A716.

Yamaki, Jun-ichi., Shinjo, Yohei., Doi, Takayuki., Okada, Shigeto., Ogumi, Zempachi., 2015. The rate equation of decomposition for electrolytes with LiPF₆ in Li-ion cells at elevated temperatures. *J. Electrochem. Soc.*, 162(4), A520-A530.

Ahn, WonSool., Yoon, SooKong., 2007. A study on formation and thermal decomposition kinetics of PU elastomers by dynamic DSC and TGA analysis. *Elastomer*, 42, 47-54.

Gaulupeau, B., Delobel, B., Cahen, S., Fontana, S., Herold, C., 2017, Real time mass spectroscopy analysis of Li-ion battery electrolyte degradation under abusive thermal conditions. *J. Power Sources.*, , 342 (2017) 808-815.

FAA Office of Security and Hazardous Materials Safety, 2019. Lithium batteries & lithium battery-powered devices. Electronic reference available at https://www.faa.gov/hazmat/resources/lithium_batteries/media/Battery_incident_chart.pdf (accessed 17.08.19).

Feng, Xuning., Ouyang, Minggao., Liu, Xiang., Lu, Languang., Xia, Yong., He, Xiangming., 2018. Thermal runaway mechanism of lithium ion battery for electric vehicles. *Energy Storage Mater*, 10, 246-267.

Peng, Yang., Yang, Lizhong., Ju, Xiaoyu., Liao, Baisheng., Ye, Kai., Li, Lun., Cao Bei., Ni, Yong., 2020. A comprehensive investigation on the thermal and toxic hazards of large format lithium-ion batteries with LiFePO₄ cathode. *J Hazard Mater*, 381, 120916-120916., Advance online publication.

Li, Huang., Duan, Qiangling., Zhao, Chunpeng., Huang, Zonghou., Wang, Qingsong., 2019. Experimental investigation on the thermal runaway and its propagation in the large format battery module with Li(Ni_{1/3}Co_{1/3}Mn_{1/3})O₂ as cathode, *J Hazard Mater*, 375, 241-254.